IEEE Access
Multidisciplinary | Rapid Review | Open Access Journal

Received February 16, 2021, accepted February 21, 2021, date of publication February 26, 2021, date of current version March 9, 2021.

Digital Object Identifier 10.1109/ACCESS.2021.3062393

Proposal of Relative Thermal Sensation: Another Dimension of Thermal Comfort and Its Investigation

ZIYANG WANG, HIROSHI ONODERA, AND RYUJI MATSUHASHI
Department of Electrical Engineering and Information Systems, The University of Tokyo, Tokyo 113-8656, Japan
Corresponding author: Ziyang Wang (wang@enesys.t.u-tokyo.ac.jp)

This work was supported in part by the Center of Innovation Stream of the Japan Science and Technology Agency.

ABSTRACT Real-time thermal comfort evaluation is not only essential in constructing the control module of Heating, Ventilation and Air Conditioning (HVAC) systems in residential buildings but also rather critical in energy conservation. In the transient thermal environment, current thermal comfort is not stable and varies from time to time. Therefore, if we only evaluate the current thermal sensation that will cause prediction error. Existing thermal comfort models mainly focus on the evaluation of current thermal comfort. However, research on the evaluation of thermal sensation variation trend is vacant. Furthermore, since individual differences play an important role in thermal comfort evaluation, physiological indices should be considered. To solve this problem, in this paper, the authors exclusively propose the concept of relative thermal sensation which accounts for the thermal sensation variation trend and give its real-time evaluation method by analysis of skin/clothes temperatures of ten local body segments using machine learning algorithms. By incorporating the relative thermal sensation model with an ordinary thermal comfort model, a novel complex thermal comfort model is derived, which has the ability to predict the current thermal comfort and the thermal sensation variation trend simultaneously and provides an early warning mechanism for thermal discomfort.

INDEX TERMS Thermal comfort evaluation, HVAC control, physiological index, skin temperature, transient thermal environment, relative thermal sensation, individual difference, machine learning, energy conservation.

NOMENCLATURE

TSV	Thermal Sensation Vote
RTS	Relative Thermal Sensation
3-point RTSS	3-point Relative Thermal Sensation Scale
RTSV	Relative Thermal Sensation Vote
ATS	Absolute Thermal Sensation
7-point ATSS	7-point Absolute Thermal Sensation Scale
ATSV	Absolute Thermal Sensation Vote
3-point TCS	3-point Thermal Comfort Scale
TCL	Thermal Comfort Level
9-point TTCS	9-point Transient Thermal Comfort Scale
TTCL	Transient Thermal Comfort Level
HVAC	Heating, Ventilation and Air Conditioning
ASHRAE	American Society of Heating, Refrigerating and Air-conditioning Engineers
MLP	Multi-layer Perceptron
RF	Random Forest

The associate editor coordinating the review of this manuscript and approving it for publication was Mouloud Denai.

I. INTRODUCTION

A. THERMAL COMFORT EVALUATION BY PHYSIOLOGICAL INDICES

Thermal comfort evaluation has become a hot topic in recent years. The ASHRAE Standard 55-2017 [1], published by the American Society of Heating, Refrigerating and Air-Conditioning Engineers (ASHRAE), defined thermal comfort as ''the condition of mind that expresses satisfaction with the thermal environment and is assessed by subjective evaluation'' [1].

Thermal comfort evaluation is essential in optimizing thermal comfort and constructing the control module of Heating, Ventilation and Air Conditioning (HVAC) systems in residential buildings and rather critical in energy conservation [2]–[4]. Empirical formulas based models such as the Precited Mean Vote/Predicted Percentage of Dissatisfied (PMV/PPD) method [5]–[9] have the ability to predict the averaged thermal comfort over a large majority of people. However, the PMV/PPD method lacks the ability to account for individual differences. Physiological factors,

including local body temperatures [10]–[13], heart rate variability (HRV) [14]–[17], pupil dilation [18], [19], et cetera, have been proved to have substantial impacts on thermal comfort, which are essential in establishing personalized thermal comfort models. Nowadays, with the rapid developing speed of technology, physiological measurement is becoming easier and easier, and the cost is becoming lower and lower. For example, the human body surface temperature can be measured by portable and low-cost infrared cameras. Many existing studies have investigated to use infrared thermography to measure body surface temperature to make thermal comfort evaluations [20]–[23].

B. TRANSIENT-STATE THERMAL COMFORT ANALYSIS

Many existing studies have focused on steady-state thermal comfort evaluation [24]–[27]. However, in the real world, people often encounter thermal discomfort under transient thermal environments rather than steady-state thermal conditions [21], [28], [29]. Steady-state thermal comfort maintenance is relatively easy. For instance, suppose an occupant feels uncomfortable under steady-state thermal conditions. In that case, there is a high possibility that he/she would simply adjust the indoor temperature according to subjective thermal sensation through the air-conditioner and finally reach a comfortable state. However, when people are in transient thermal environments, the thermal sensation is not stable and varies from time to time, thus following the current thermal sensation to control the HVAC system is not reliable. For instance, suppose an occupant walks into a sauna room, he/she might feel comfortably warm at first. However, as time goes by, the occupant might feel uncomfortably hot at last. Oppositely, suppose an occupant is walking out from a well-heated house in the winter season, the occupant may feel comfortably cool at first. However, as time goes by, he/she may finally feel uncomfortably cold. Therefore, transient-state thermal comfort evaluation becomes much more important and challenging than steady-state thermal comfort evaluation.

For transient-state thermal comfort analysis, Li *et al.* [30] developed a thermal comfort model based on facial skin temperature measured by infrared thermography under heating (22 °C-28 °C) and cooling (28 °C-22 °C) conditions. Choi and Yeom [12] developed a thermal comfort model based on skin temperatures of local body segments measured by an exposed thermistor type sensor under heating (20 °C-30 °C) and cooling (30 °C-20 °C) conditions. However, the air temperature change rates in these studies were too low to simulate a transient thermal environment, e.g., 1 °C/10 minutes [12], [30], resulting in a reasonable doubt on the fast response capability of these thermal comfort models under rapid air temperature change scenarios.

C. LIMITATIONS OF THE ASHRAE 7-POINT THERMAL SENSATION SCALE

Thermal Sensation Vote (TSV), is the vote on thermal sensations reported by people. The ASHRAE Standard 55 [1], [29], [31], [32] defined 7-point thermal sensation scale has seven categories starts from −3 to +3, corresponding to "cold," "cool," "slightly cool," "neutral," "slightly warm," "warm," and "hot."

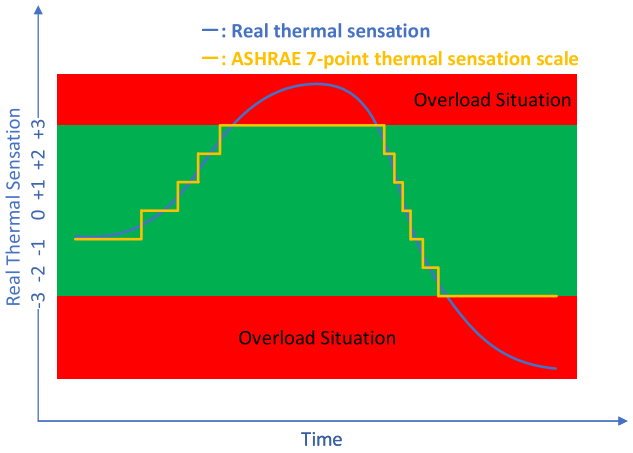

FIGURE 1. Schematic of the overload situation of the ASHRAE 7-point thermal sensation scale.

Two problems appear here. First, since the ASHRAE 7-point thermal sensation scale has an upper limit (+3) and a lower limit (−3), when the real thermal sensation exceeds the upper limit or the lower limit, the ASHRAE 7-point thermal sensation scale will be overloaded, as illustrated in Fig. 1. Second, since the ASHRAE 7-point thermal sensation scale is discrete, it cannot describe the thermal sensation details when the thermal sensation fluctuates within a certain level of the ASHRAE 7-point thermal sensation scale and cause information loss, as illustrated in Fig. 1. In Fig. 1, the continuous blue curve indicates the real thermal sensation whereas the orange polygonal line indicates the discrete TSV based on the ASHRAE 7-point thermal sensation scale. Moreover, in the subjective thermal sensation acquisition process in existing thermal comfort evaluation studies, the time interval for TSV was relatively long, e.g., fifteen minutes [33], five minutes [12], [34], three minutes [30], or one minute [21], [22], thus causes a negative impact on the real-time performance of the models.

II. METHODOLOGY

A. THE CONCEPT OF RELATIVE THERMAL SENSATION

In traditional ASHRAE 7-point thermal sensation scale, the thermal sensation is discrete. In contrast, in this study, the occupant's real thermal sensation is considered to be continuous. If we consider the thermal sensation to be a continuously differentiable function $f(t)$ of time t, then at time t_0, $f(t)$ can be written in the Taylor series, as is shown in (1).

$$f(t) = f(t_0) + \frac{f'(t_0)}{1!}(t - t_0) + \frac{f''(t_0)}{2!}(t - t_0)^2 + \ldots, \quad (1)$$

$$f(t) \approx f(t_0) + f'(t_0)(t - t_0) \quad (2)$$

According to Taylor's theorem, the linear approximation of $f(t)$ for t near t_0 is shown in (2). In (2), the first term $f(t_0)$

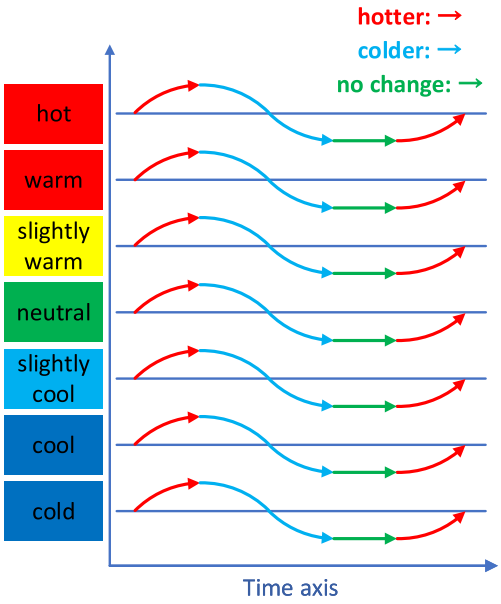

FIGURE 2. Schematic of the Relative Thermal Sensation (RTS).

is the exact thermal sensation degree at t_0. The coefficient of the second term $f'(t_0)$, describing the gradient of the thermal sensation, is precisely defined as the Relative Thermal Sensation (RTS) in this study. In this paper, the authors exclusively propose the concept of RTS and its real-time evaluation method. Next, the 3-point Relative Thermal Sensation Scale (3-point RTSS) for gathering the Relative Thermal Sensation Vote (RTSV) reported by the occupants for the RTS evaluation is proposed. For the sake of simplification, the 3-point RTSS is defined to be discrete and consists of three categories "hotter," "colder," and "no change." Each category is called an RTSV. The RTSV is defined as "hotter" when the occupant's current thermal sensation is hotter than the latest thermal sensation (when $f'(t) > 0$); the RTSV is defined as "colder" when the occupant currently feels colder than the latest thermal sensation (when $f'(t) < 0$); when the occupant's current thermal sensation does not change compared with the latest thermal sensation (when $f'(t) = 0$), the RTSV is defined as "no change." The 3-point RTSS can serve as a complementary thermal sensation index for the traditional ASHRAE 7-point thermal sensation scale for transient-state thermal comfort evaluation, as illustrated in Fig. 2. Fig. 2 shows the schematic diagram of the RTS. In Fig. 2, the left part shows the ASHRAE 7-point thermal sensation scale, and the thick continuous curves indicate the occupant's real thermal sensation. The "hotter" periods, "colder" periods, and "no change" periods are depicted in red, blue, and green, respectively. Note that the definition of "hotter" not only describes the transition from "warm" to "hot," but also covers the transition from "cold" to "cool." The same to the definition of "colder." The concept of the 3-point RTSS sounds similar to the McIntyre 3-point thermal preference scale (MCI) [13] but fundamentally different. The McIntyre Index is defined as: "At this point in time, would you prefer to feel warmer, cooler, or no change? [7]" The McIntyre Index emphasizes the thermal preference, whereas the 3-point RTSS describes the real-time thermal sensation variation trend.

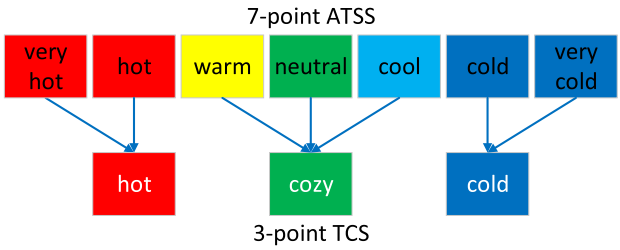

FIGURE 3. 7-point Absolute Thermal Sensation Scale (7-point ATSS) and the 3-point Thermal Comfort Scale (3-point TCS).

Except for using the ASHRAE 7-point thermal sensation scale exclusively, researchers modify the ASHRAE 7-point thermal sensation scale or define their own thermal sensation scales in a variety of case studies [35]–[38]. In [33], Ghahramani *et al.* used "comfortably warm" and "comfortably cool" to express comfortable thermal states. To better distinguish from the RTS and the 3-point RTSS, in this study, similarly with [33], the authors denominate the thermal sensation in the common sense $f(t_0)$ in (2) as the Absolute Thermal Sensation (ATS). Also, the authors modify the ASHRAE 7-point thermal sensation scale and give it a new name: 7-point Absolute Thermal Sensation Scale (7-point ATSS), as shown in Fig. 3. The 7-point ATSS has seven categories "very hot," "hot," "warm," "neutral," "cool," "cold," and "very cold." Each category is called an Absolute Thermal Sensation Vote (ATSV). The "warm," "neutral," and "cool" votes in the 7-point ATSS are defined to represent the comfortably cozy state; the "hot" and "very hot" votes express the uncomfortably hot state; the "cold" and "very cold" votes express the uncomfortably cold state. By such a definition, the 3-point Thermal Comfort Scale (3-point TCS) can be derived from the 7-point ATSS, as illustrated in Fig. 3. The 3-point TCS has three categories "hot," "cozy," and "cold." Each category in the 3-point TCS is called a Thermal Comfort Level (TCL).

Suppose the RTS can be evaluated accurately, it will be very beneficial in predicting the next TCL when given the current TCL. By incorporating the 3-point TCS and the 3-point RTSS together, we can obtain the 9-point Transient Thermal Comfort Scale (9-point TTCS), which is a complex model and has the ability to describe both thermal comfort and thermal sensation variation trend simultaneously, as described in Fig. 4. The 9-point TTCS has nine categories "hot to hot," "hot," "hot to cozy," "cozy to hot," "cozy," "cozy to cold," "cold to cozy," "cold," and "cold to cold." Each category in the 9-point TTCS is called a Transient Thermal Comfort Level (TTCL). For instance, in winter, suppose an occupant stays in an air-conditioning room with the heating system working on, and the occupant's current TCL is "cozy." Meanwhile, if the occupant's RTS is "hotter," the TTCL will be

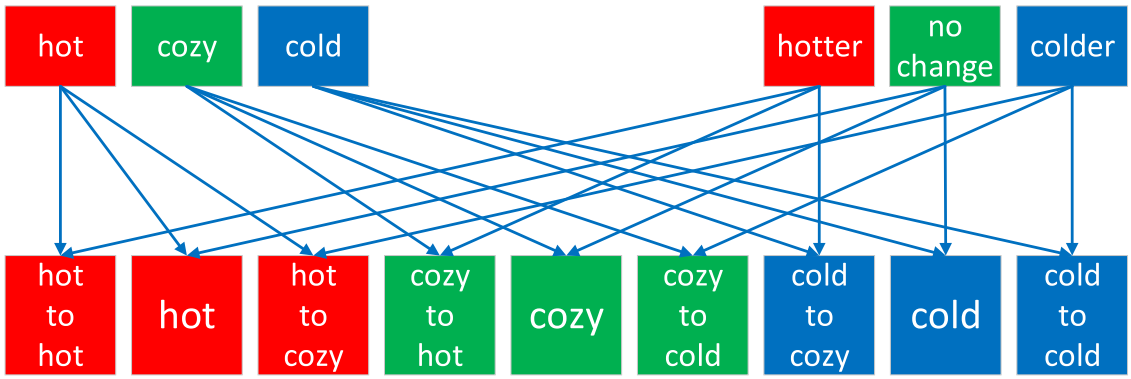

FIGURE 4. 9-point Transient Thermal Comfort Scale (9-point TTCS) generated by incorporating the 3-point RTSS into the 3-point TCS.

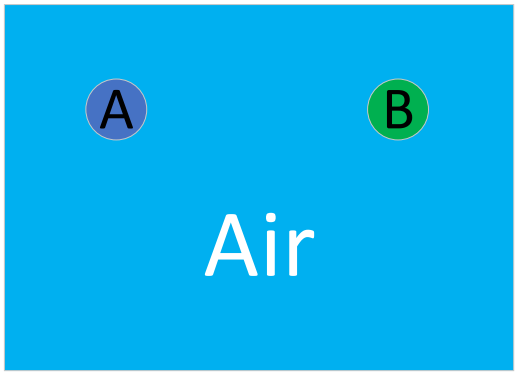

FIGURE 5. Idea illustration.

"cozy to hot". It means that we can reasonably infer that the occupant's next TCL may transit from "cozy" to "hot" if the heating system proceeds to work on. In that case, it would be better to stop heating the room to maintain the "cozy" TCL. On the other hand, if the TTCL were "hot to hot", it means that the degree of discomfort (hot) of the occupant will aggravate by the next time point. Note that in the 9-point TTCS, since the "hot," "cozy," and "cold" are generated by incorporating the "no change" RTS into the 3-point TCS, they are considered to be instant steady TCL. If the TTCL can be assessed accurately, it will be very beneficial to help to avoid running into an uncomfortable TCL in advance. Not only the thermal comfort can be ensured, but also the energy will be saved.

B. DIFFERENT MATERIALS HAVE DIFFERENT THERMAL PROPERTIES

As is known to all, different materials have different thermal properties, such as heat conductivity, specific heat capacity, et cetera. Fig. 5 shows a typical example of the main idea in this study.

In Fig. 5, suppose we have two small particles, A and B, surrounded by the air, and the system is in a steady-state thermal environment. Suppose particles A and B have the same shape, same size, and same heat conductivity while the specific heat capacity of particle A is higher than the specific heat capacity of particle B, and the initial temperatures of particles A and B are the same. When the air temperature starts to fluctuate uniformly, on account of the relatively higher specific heat capacity of particle A, there will generate a temperature difference between particles A and B. When the air temperature starts to ascend, the temperature of particle B will be higher than the temperature of particle A; when the air temperature starts to descend, the temperature of particle B will be lower than the temperature of particle A; when the air temperature does not change, the temperature of particle A and the temperature of particle B will be equal. Hence, the variation trend of the air temperature can be inferred by the temperature difference of particle A and particle B.

The lemma mentioned above illustrates the simplest case. Generally speaking, when the air temperature increases, people tend to feel "hotter"; when the air temperature decreases, people tend to feel "colder." However, things are much more complicated in the real world that only by comparing the temperature of two particles in the thermal environment to identify people's RTS may cause a mistake. The idea is to promote the scenario from two particles into multiple points that lie on a more generalized two-dimensional curved surface, e.g., the human body surface, as illustrated in Fig 6. Furthermore, intuitively, the body surface temperature gradient may also play an important role in determining the RTS.

According to [39], the specific heat capacity of the tissues in skin layers plays an important role in preventing the deeper tissues from thermal damage, which indicates that the heat capacity distribution of human skin varies from location to location. Also, in [40], Kashcooli *et al.* pointed out that the distribution of blood vessels has an essential impact on skin temperature distribution. Also, due to the geometrical structure of the human body, some specific body regions are protruding from the body trunk, and the blood vessel distribution density in which tends to be lower than the body trunk, for instance, the legs, the feet, hands, ears, and nose. Thus, the temperature in such areas may be more easily affected by air temperature than in other areas. Moreover, as for the body surface areas covered with clothes, the heat property

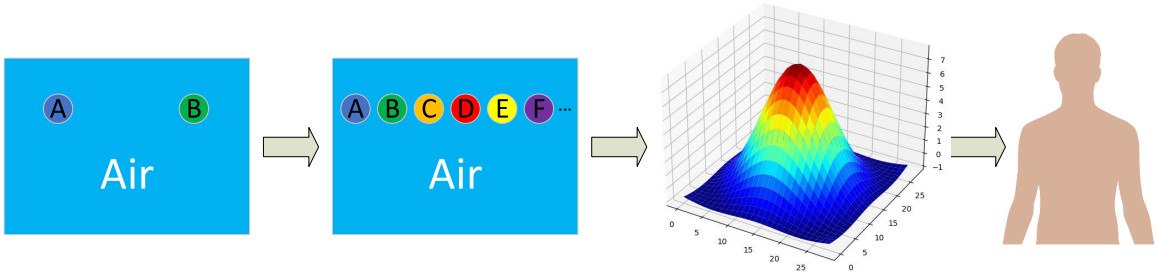

FIGURE 6. Promotion from two particles to a surface.

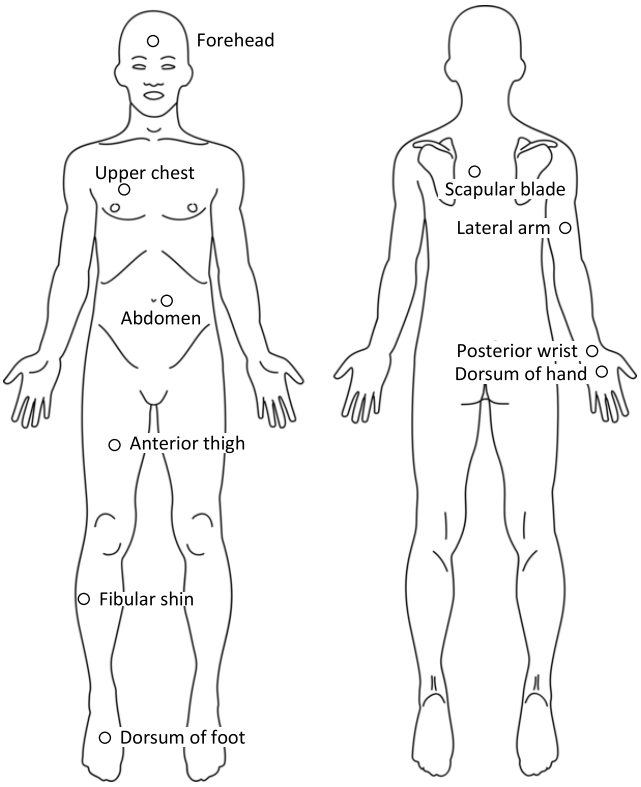

FIGURE 7. Schematic of the body locations selected in the investigation.

should also vary from location to location. From the above, the hypothesis is that different RTS corresponds to different specific body surface temperature distribution, and the RTS can be assessed by analyzing skin/clothes temperatures of local body segments and subjective RTSV data by utilizing machine learning classification algorithms.

C. EXPERIMENTAL DESIGN

The authors conducted an experiment to verify the hypothesis. In [12], Choi *et al.* investigated the relationship between local skin temperatures of the upper body and the TSV under a slow air temperature variation scenario (1 °C/10 minutes). In this study, in order to acquire an overall temperature distribution of the whole body, the authors selected ten local body segments not only covering the upper body but also including the lower body from a thermal mannequin schematic in [41]

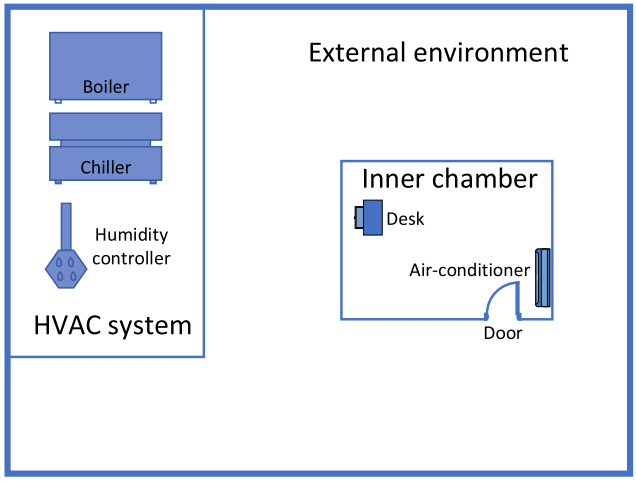

FIGURE 8. Schematic of the environmental test lab.

to investigate the skin/clothes temperatures under transient thermal environments. The local body segments include the forehead, the upper chest, the lateral arm, the dorsum of the hand, the abdomen, the scapular blade, the anterior thigh, the fibular shin, and the dorsum of the foot, as shown in Fig. 7. According to [12], [42], wrist skin temperature has a strong impact on thermal comfort. Apart from the nine locations derived from [41], the authors also added the posterior wrist into the investigation, as shown in Fig. 7.

The experiment was conducted in the environmental test lab of Tokyo Gas Co., Ltd. in the winter season, February 2020. The environmental test lab consists of an external environment and an inner chamber, as illustrated in Fig. 8. There is an HVAC system inside the external environment. The HVAC system is equipped with a boiler, a chiller, and a humidity controller. The HVAC system controls the air temperature and humidity of the external environment to maintain the preset degree. The inner chamber has an air-conditioner installed to adjust the air temperature inside the inner chamber. Moreover, the inner chamber has a door to allow for ventilation through the external environment. Due to the fact that the external environment is much larger than the inner chamber, the temperature variation of the external environment can be neglected when opening the door of the inner chamber to make heat exchange.

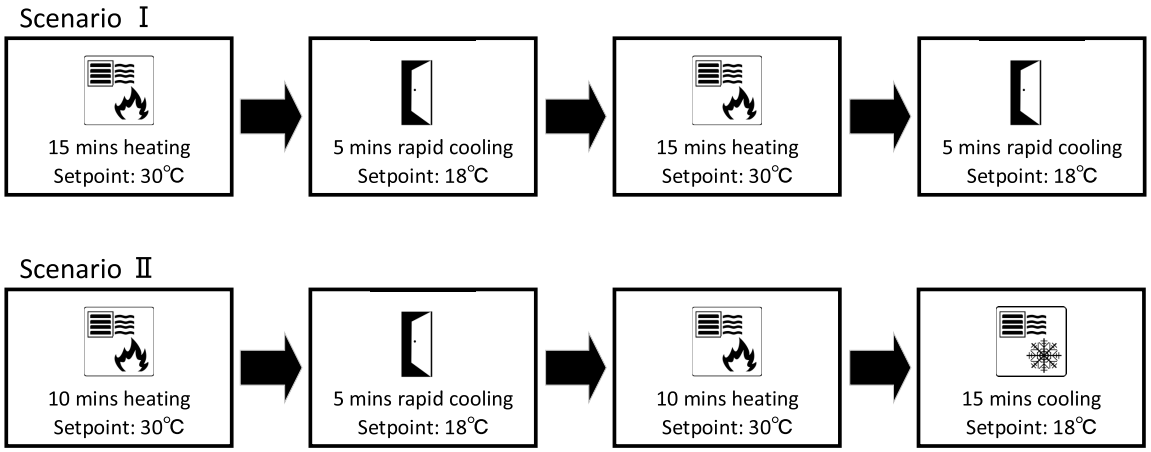

FIGURE 9. Temperature control schemes of the inner chamber.

The authors used two temperature control schemes to simulate two different scenarios, as is described below. During the experiment, the temperature and humidity of the external environment were adjusted to 18°C and 50%, respectively.

1) SCENARIO I

Due to the fact that the inner chamber allows for ventilation from the external environment through the door, the authors utilized this feature to simulate a rapid temperature variation scenario. The temperature control scheme of the inner chamber is described in Fig. 9. The whole procedure consists of two identical gradual heating phases and two identical rapid cooling phases. In the first phase, close the door and turn on the heating mode of the air-conditioner in the inner chamber to gradually heat the room for 15 minutes, the setpoint was chosen as 30 °C. The 15-min-long heating phase is relatively long enough to heat the room and make the room temperature level off during the latter half of the heating phase. In the second phase, turn off the air-conditioner and open the door for 5 minutes. As a consequence, the air temperature of the inner chamber will be drastically decreased approximately to the temperature of the external environment through the heat exchange with the external environment and will then level off and fluctuate up and down within a small range. By repeating the aforementioned two phases, a periodic temperature signal with a period of 20 minutes can be generated. The total duration of the experiment is 40 minutes. In both heating and cooling phases, the air temperature is supposed to be adjusted to an area where it does not rise or fall significantly. The authors intended to investigate the RTS and ATS behaviours under such a thermal condition. The RTS is supposed to change when the inner chamber is sufficiently cooled or heated.

2) SCENARIO II

This Scenario also consists of two identical gradual heating phases and two cooling phases, as described in Fig. 9. Different from Scenario I, the authors added a gradual cooling phase in Scenario II. In the heating phases, close the door and turn on the heating mode of the air-conditioner in the inner chamber, the setpoint was chosen as 30 °C. The first cooling phase is the rapid cooling phase in which the door was opened to make heat exchange with the external environment for 5 minutes. The second cooling phase is the gradual cooling phase in which the air-conditioner was utilized to cool the inner chamber, and the setpoint was chosen as 18 °C to keep consistent with the air temperature of the external environment. The duration of the gradual cooling phase was set to 15 minutes long to ensure the air temperature to be lowered approximately to 18 °C by the end of the cooling phase. In addition, the duration of either of the two heating phases was shortened to 10 minutes to keep the total experiment duration to 40 minutes to keep consistent with Scenario I. The intention of adding the rapid cooling phase and the gradual cooling phase together is to verify the applicability of the proposed machine learning model for the RTS evaluation under completely different cooling schemes.

D. EXPERIMENTAL PROCEDURE

The two scenarios mentioned above were randomly selected and applied in the experiment. Six male students (age 25 ± 1 years) at the University of Tokyo participated in the experiment. Three subjects were applied to Scenario I, and the other three were applied to Scenario II.

Before the experiment, the door was kept open to keep the inner chamber air temperature approximately equal to the air temperature of the external environment. The subjects were requested to wear the same clothes (black short sleeves, trousers, and cotton socks) and sit down on the pre-prepared chair during the experiment. A laptop for the TSV input was set on a desk in front of the chair. The desk and the chair were arranged not to front the wind from the air-conditioner or the door directly, as illustrated in Fig. 8. The subjects put their feet on a pre-prepared thermal insulation pad to

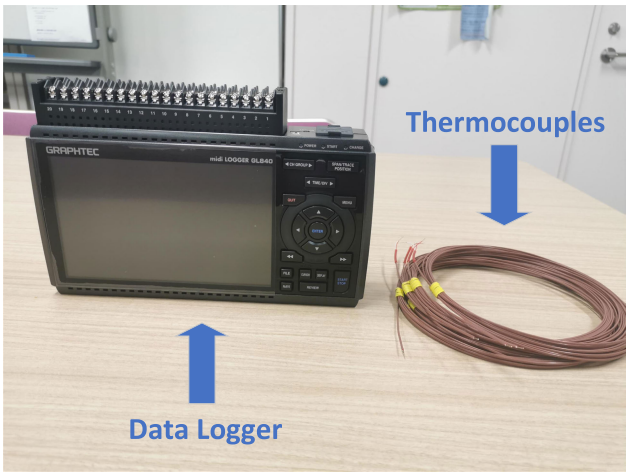

FIGURE 10. Midi LOGGER GL840.

prevent unnecessary conductive heat loss through the floor. The subjects were requested to sit down on the chair before the experiment for preparation to maintain a "no change" RTS (steady state). Before the experiment starts, the subjects were asked to confirm whether their current RTSV is "no change" or not.

During the preparation time (20 minutes), the thermocouples were fixed to the subjects' specific local body segments. At the local body segments of the forehead, the lateral arm, the posterior wrist, and the dorsum of the hand, skin surface temperatures were measured. Whereas at the local body segments of the upper chest, the abdomen, the scapular blade, the anterior thigh, the fibular shin, and the dorsum of the foot, clothes surface temperatures were measured. The temperature data were recorded by a data logger (Midi LOGGER GL840: Accuracy: ± 0.5 °C, Resolution: 0.01 °C) and thermocouples (Type T (copper-constantan)) per second with accurate temporal synchronization, as shown in Fig. 10. The authors used a medical tape to fix the thermocouples onto the skin surface, or the clothes surface, as shown in Fig. 11. While fixing the thermocouples onto the clothes surface, loose areas were avoided to keep the thermocouples stable. In general, mesial body parts were not considered. Since mesial body parts usually rub against other body parts, when it comes to the real application of using skin/clothes temperatures of local body segments to predict thermal comfort, installing sensors on such body locations may cause uneasiness and inaccuracy. The ambient air temperature was measured per second by a thermocouple placed 60 cm above the floor near the subject. Fig. 11 shows the whole experimental setup. The subjects were not aware of the operation of the air-conditioner and the opening/closing of the door and were requested to vote the thermal sensation according to subjective feelings. The experiment was approved by the Research ethics committee of the University of Tokyo.

E. THERMAL SENSATION VOTE INPUT SYSTEM

A laptop was used for real-time TSV input. Table. 1 shows the keyboard buttons corresponding to the RTSV and ATSV.

FIGURE 11. Experimental setup.

TABLE 1. TSV input rule.

keyboard button	TSV	Category	Priority
1	very cold	ATSV	ATSV > RTSV
2	cold		
3	cool		
4	neutral		
5	warm		
6	hot		
7	very hot		
↑	hotter	RTSV	
↓	colder		

Fig. 12 shows the keyboard layout for the RTSV and ATSV input. The input rule is described in Table. 1. As this study is focused on real-time transient-state thermal comfort evaluation, it is important to gather as much thermal sensation details as possible. In fact, instead of inputting the RTSV and ATSV exactly at a series of equally spaced time points, the subjects were encouraged to instantly input the RTSV and ATSV whenever they feel a thermal sensation change. However, minimally, the subjects were requested to input the TSV (RTSV or ATSV) once at least every 20 seconds. There was an alarm clock program installed in the laptop ringing every 20 seconds as a reminder. When hearing the alarm, the subjects press the keyboard button instantly. Note that the priority of the ATSV is higher than the priority of

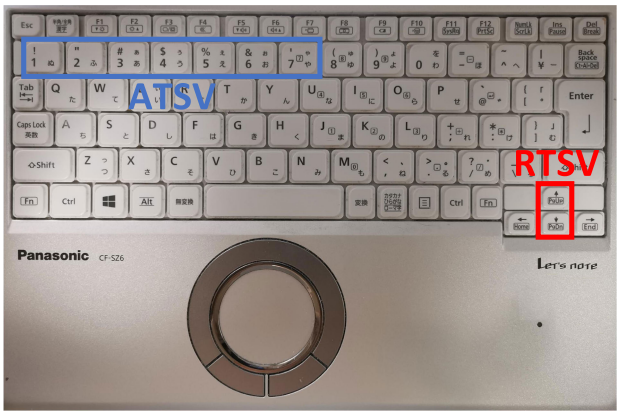

FIGURE 12. Keyboard layout for the TSV input.

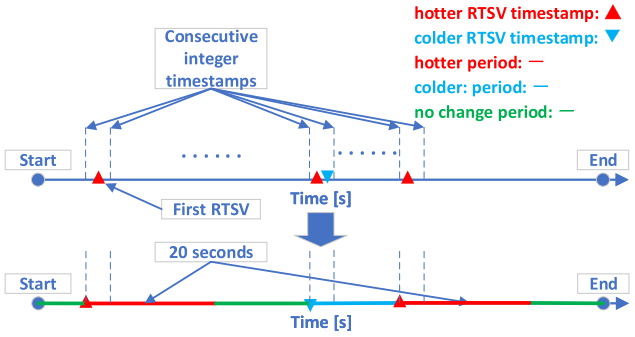

FIGURE 13. Schematic of the RTSV processing method.

the RTSV. Concretely, if the subject feels a distinct thermal sensation change in the 7-point ATSS, e.g., from "cool" to "cold," the subject should press the keyboard button "2" rather than press the keyboard button "down" exclusively; if the former ATSV is "cool" and the current ATSV is also "cool", but the current "cool" sensation is colder than the previous "cool" sensation, the subject should press the "down" keyboard button. That is to say, a transitioning from one ATSV to another ATSV will also be counted to the RTS. The timestamp of recording the pressings of the keyboard button has a resolution of 0.001 seconds. The "hotter" and "colder" RTSV were regarded to sustain 20 seconds long after the input to keep consistent with the TSV input interval when there is no successive "hotter" or "colder" RTSV within 20 seconds. To alleviate the subjects' burden, the authors did not set the "no change" RTSV as an active vote in this investigation, time periods with no "hotter" or "colder" RTS were regarded as the "no change" periods.

The RTSV data processing method is illustrated in Fig. 13. For the RTSV data, the authors set the resolution of the time axis of the RTS to one second to keep consistent with the temperature data by rounding down the RTSV timestamps to the nearest integers (e.g., 12.632 seconds → 12 seconds). When there are multiple RTSV within one second, only the last RTSV will be reserved. Next, complement the sustaining "hotter" and "colder" periods. Finally, complement the "no change" periods. The time interval between the start time and

Algorithm 1 Calculate Local Body Temperature Difference

Input: $LBT_i(t), i = 1, \ldots, n$
Output: $LBTD(t)$

```
LBTD(t) ← Empty List
for i ← 1 to n do
    for j ← 1 to n do
        if j ≠ i ∩ j > i then
            LBTD_ij(t) = LBT_i(t) − LBT_j(t)
            LBTD(t).append(LBTD_ij(t))
        end if
    end for
end for
return LBTD(t)
```

the first RTSV timestamp was regarded as the "no change" period. For the ATSV data, the ATS between the start time and the first ATSV timestamp was considered the same as the first ATSV; the ATS between the end time and the last ATSV timestamp was considered the same as the last ATSV. Then the authors applied linear interpolation to the ATSV data with a time interval of one second. Then round the ATS to the nearest integers. Finally, based on Fig. 3, the TCL data can be obtained from the ATS data.

F. RTS AND TCL EVALUATION BY MACHINE LEARNING

1) FEATURE EXTRACTION FOR RTS EVALUATION

In the RTS evaluation, the temperature differences between one reference local body segment and all the other segments were extracted as features according to the hypothesis mentioned above. The pseudo-code for calculating the temperature differences is described as follows.

Here, the input series $LBT_i(t), i = 1, \ldots, n$ is each of the local body segment temperatures, i is the serial number of each local body segment, n is the number of local body segments, t is the sampling time. Since we selected ten local body segments in this experiment, n was set to 10. Since the temperature was measured per second, and the total duration of the experiment was 40 minutes, 2400 samples were obtained for each subject. The $LBTD_{ij}(t)$ is the temperature difference between local body segment i and local body segment j. Consequently, 45 temperature differences were generated for each timestamp and were appended to the $LBTD(t)$.

Next, the moving average smoothing method was applied to the $LBT_i(t)$ and $LBTD_{ij}(t)$ to extract the smoothed $LBT_i(t)$ and $LBTD_{ij}(t)$ as features. The calculation method is shown in (3) and (4). The $\overline{LBT_i(t)}$ and $\overline{LBTD_{ij}(t)}$ are the smoothed $LBT_i(t)$ and $LBTD_{ij}(t)$, respectively. The window size was set to 20 seconds to keep consistent with the TSV input interval.

$$\overline{LBT_i(t)} = \sum_{\tau=-10}^{\tau=9} LBT_i(t+\tau), \quad i = 1, \ldots, n \tag{3}$$

$$\overline{LBTD_{ij}(t)} = \sum_{\tau=-10}^{\tau=9} LBTD_{ij}(t+\tau), \quad i, j = 1, \ldots, n, \quad j \neq i \cap j > i \tag{4}$$

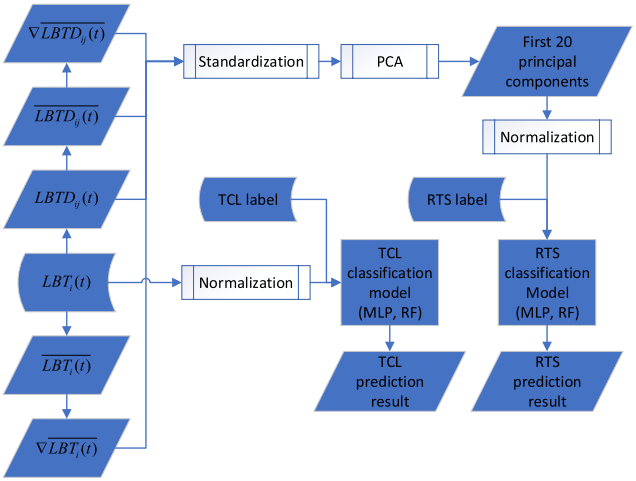

FIGURE 14. Data processing pipeline for the RTS and TCL classifications.

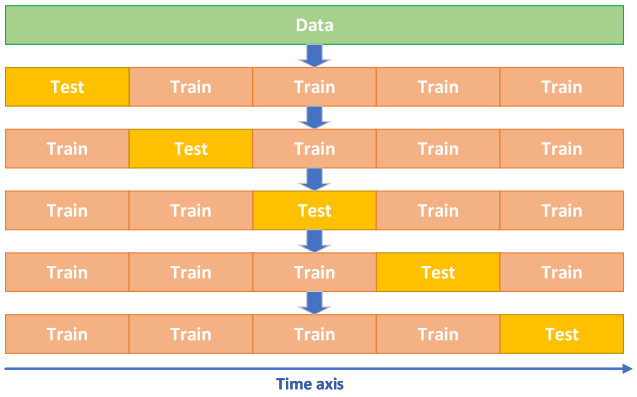

FIGURE 15. Training and test set separation.

Next, the gradients of the $\overline{LBT_i(t)}$ and $\overline{LBTD_{ij}(t)}$ were extracted as features. The calculation method is shown in (5) and (6). The interval for calculating the difference was set to 5 seconds. The $\nabla\overline{LBT_i(t)}$ and $\nabla\overline{LBTD_{ij}(t)}$ are the gradients of the $\overline{LBT_i(t)}$ and $\overline{LBTD_{ij}(t)}$, respectively.

$$\nabla\overline{LBT_i(t)} = \overline{LBT_i(t)} - \overline{LBT_i(t-5)}, \quad i = 1, \ldots, n \tag{5}$$

$$\nabla\overline{LBTD_{ij}(t)} = \overline{LBTD_{ij}(t)} - \overline{LBTD_{ij}(t-5)}, \quad i, j = 1, \ldots, n, \quad j \neq i \cap j > i \tag{6}$$

2) FEATURE EXTRACTION FOR RTS EVALUATION USING PRINCIPAL COMPONENT ANALYSIS (PCA)

In fact, some features extracted above are highly correlated and redundant since the original skin/clothes temperatures of different local body segments may have a very similar variation trend, such as the abdomen temperature and the shin temperature as shown in Fig. 17 and Fig. 18, thus causing the multicollinearity issue. This problem is usually solved by the principal component analysis (PCA). As an unsupervised learning technique, the PCA projects the data onto a relatively low-dimensional space and is a common feature extraction method to address the multicollinearity issue. The authors carried out a PCA test using the Python Scikit-learn package. The $LBTD_{ij}(t)$, the $\overline{LBTD_{ij}(t)}$, the $\nabla\overline{LBT_i(t)}$, and the $\nabla\overline{LBTD_{ij}(t)}$ were standardized and inputted to the PCA model together for feature extraction. Instead of using the features extracted above directly, the first 20 principal components from the PCA output were used as the input of the RTS classification model after normalization.

3) RTS AND TCL CLASSIFICATIONS

Fig. 14 shows the data processing pipeline for the RTS and TCL classifications. In the RTS evaluation, the first 20 principal components from the PCA output were used as the input of the RTS classification model after normalization. In the TCL evaluation, the authors used a mediocre method in which the skin/clothes temperatures of the ten local body segments ($LBT_i(t)$) were simply used as the input of the TCL classification model since it was not the key point of this investigation. The outputs of the RTS and TCL classification models are the RTS prediction and the TCL prediction, respectively.

The authors utilized a Multi-layer Perceptron (MLP) classifier and a Random Forest (RF) classifier to make predictions of the RTS and the TCL for each subject. The MLP classifier and the RF classifier were trained using the Python Scikit-learn package. Optimal hyper-parameters of the MLP and RF classifiers in the RTS and TCL classifications were obtained using the grid search technique (MLP classifier: 'hidden_layer_sizes': [(4,), (6,), (8,), (10,), (12,), (14,), (16,), (18,), (20,), (30,), (40,), (50,)], 'max_iter'=200, 'alpha': [0.0001, 0.05], 'learning_rate': ['constant', 'adaptive'], 'solver': ['sgd', 'adam']. RF classifier: 'n_estimators': [100, 300, 500, 700, 900, 1100], 'max_features': ['auto', 'sqrt', 'log2'], 'max_depth': [2, 3, 4, 5, 6]). Due to the limited data capacity, to make full use of all the data, the authors carried out the 5-fold cross-validation without shuffling suggested by [43], in which the data samples of each subject were equally partitioned into five equal-sized segments according to chronological order. Then by iterating the process of using four segments as the training set and using the remaining one segment as the test set, as illustrated in Fig. 15, every segment will be used as the test set once and generates the prediction. By combining all the predictions generated by all the segments, the whole prediction can be obtained. The TTCL prediction then can be generated by incorporating the RTS prediction into the TCL prediction.

III. RESULTS

The air temperature conditions in the four phases of the inner chamber are summarized in Table. 2. In Scenario I, the standard deviations of the air temperature in both cooling phases are lower than that in both heating phases since the temperature dropped rapidly and leveled off in both cooling phases. In Scenario II, the standard deviation of the air temperature in the second cooling phase is higher than that in the first cooling phase, close to that in both heating phases since the air temperature dropped slowly in the second cooling phase.

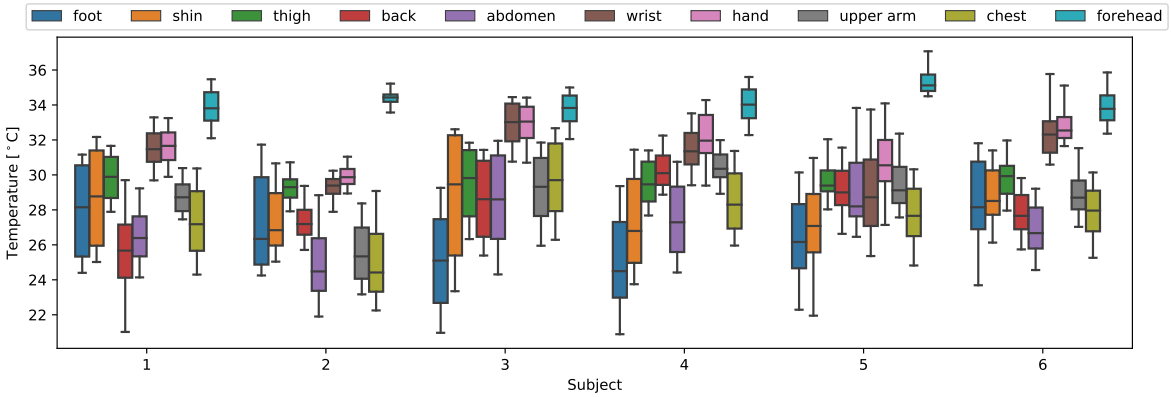

FIGURE 16. Boxplot of local body segment temperatures for all subjects.

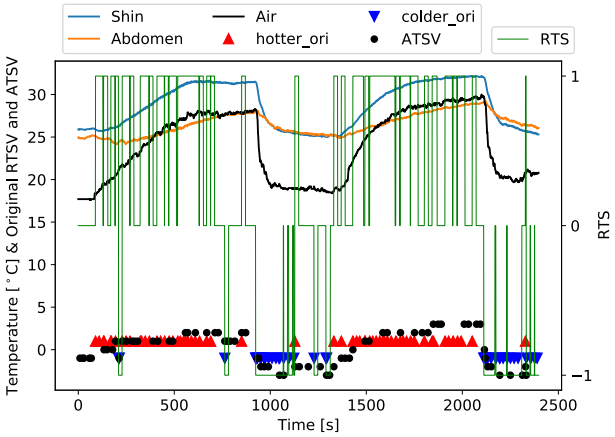

FIGURE 17. Experimental data (Scenario I & Subject 1).

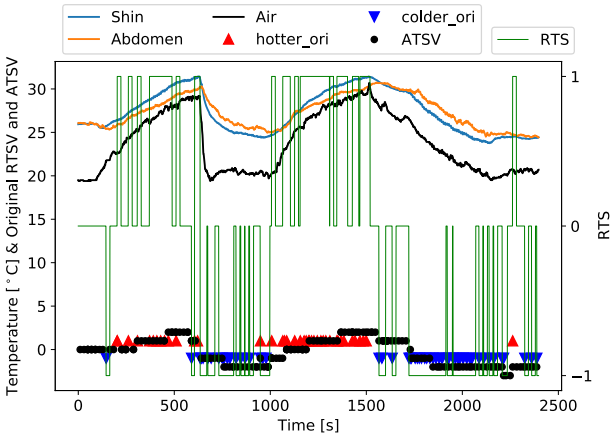

FIGURE 18. Experimental data (Scenario II & Subject 4).

Fig. 16 presents the boxplot of the temperature distributions of the ten local body segments obtained from the experiment. No obvious difference can be observed between the two scenarios. However, we can observe obvious individual differences among the subjects. In both scenarios, the clothes surface temperatures have a relatively higher variance than that measured on the skin surface since the clothes have a heat insulation effect. The forehead reached the highest temperature than other body segments; the shin and foot temperatures had a higher variance than that of the abdomen, the chest, and the back since the latter three local body segments occupy the trunk of the body while the former two local body segments are the body branches.

TABLE 2. Summary of the inner chamber temperature conditions in four phases.

Scenario	Phase	Range (°C)	Mean (°C)	S.D. (°C)
I	Heating 1	17.6-28.6	24.5	3.6
	Cooling 1	28.9-18.4	19.6	1.6
	Heating 2	18.1-30.0	26.7	3.3
	Cooling 2	29.8-19.7	21.5	1.7
II	Heating 1	19.4-29.2	24.7	3.4
	Cooling 1	28.9-19.3	20.7	1.4
	Heating 2	19.7-30.7	26.4	2.9
	Cooling 2	30.6-19.5	23.1	3.1

Fig. 17 and Fig. 18 show the representative data of two subjects from the two scenarios, including the temperature data, the original RTSV, the original ATSV, and the integrated RTS. The red triangles and inverted blue triangles indicate the original "hotter" and "colder" RTSV; the black dots indicate the original ATSV; the green line shows the integrated RTS calculated by taking the internal transitions within the ATSV into account and adding the "no change" periods. In both Fig. 17 and Fig. 18, during the periods when the subjects mostly felt "hotter," the shin temperature was higher than the abdomen temperature. In contrast, when the subjects mostly felt "colder," the shin temperature was lower than the abdomen temperature, which agrees with our hypothesis mentioned above, indicating that it could be reasonable to use local body segment temperature differences to predict the RTS.

In Fig. 17, in the first heating phase and the first cooling phase, when the air temperature leveled off for a while, short periods of RTS transitioning from "hotter" to "colder" or "colder" to "hotter" can be observed. The reason was

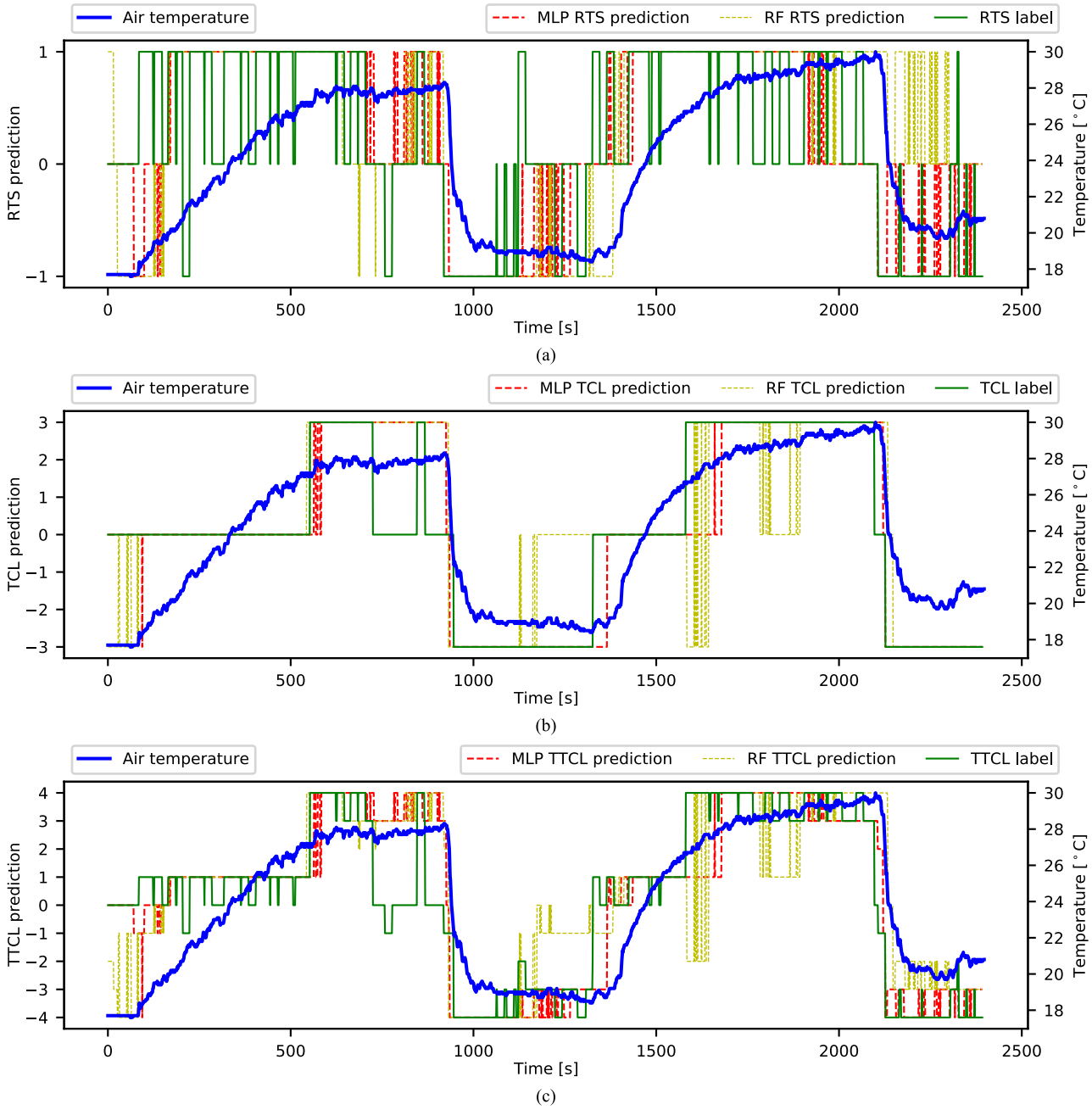

FIGURE 19. Prediction results of the RTS, the TCL, and the TTCL (Scenario I & Subject 1).

considered to be the adaptive effect according to [29]. In the first cooling phase in Fig. 18, after an abrupt air temperature drop, although the air temperature had an increment, the RTS retained to be "colder," revealing the fact that the RTS does not always comply with the air temperature variation trend.

A. RTS AND TCL CLASSIFICATION RESULTS

Table. 3 shows the correspondence of the numerical labels of the 3-point RTSS, the 3-point TCS, and the 9-point TTCS in the prediction results of the classifications. The accuracy is summarized in Table. 4. The confusion matrix, support (the number of actual occurrences of each category), precision, recall, and F1-score of the RTS classification result for all subjects are summarized in Table. 5. Fig. 19 and Fig. 20 show the prediction results of the RTS, the TCL, and the TTCL of the two subjects from Scenario I and Scenario II as mentioned above, respectively. In Scenario I, the RTS mean prediction accuracy of the MLP and RF classifiers reached 0.63 and

TABLE 3. Label references for the 3-point RTSS, the 3-point TCS, and the 9-point TTCS.

Label	3-point RTSS	3-point TCS	9-point TTCS
-4			cold to cold
-3		cold	cold
-2			cold to cozy
-1	colder		cozy to cold
0	no change	cozy	cozy
1	hotter		cozy to hot
2			hot to cozy
3		hot	hot
4			hot to hot

TABLE 4. Classification accuracy of the RTS, the TCL, and the TTCL.

Scenario	Subject	RTS		TCL		TTCL	
		MLP	RF	MLP	RF	MLP	RF
I	1	0.67	0.55	0.85	0.73	0.57	0.43
	2	0.59	0.64	0.69	0.86	0.46	0.59
	3	0.62	0.60	0.76	0.84	0.46	0.48
	Mean	0.63	0.60	0.77	0.81	0.50	0.50
II	4	0.68	0.59	0.64	0.77	0.47	0.49
	5	0.56	0.32	0.70	0.81	0.43	0.23
	6	0.55	0.52	0.84	0.80	0.46	0.43
	Mean	0.60	0.48	0.73	0.79	0.45	0.38

0.60, respectively. In Scenario II, the RTS mean prediction accuracy of the MLP and RF classifiers reached 0.60 and 0.48, respectively. The precision, recall, and F1-score of the ''hotter'' RTS and ''colder'' RTS are relatively higher than the precision, recall, and F1-score of the ''no change'' RTS in both scenarios. The MLP classifier outperformed the RF classifier in the RTS classification result.

It is noticeable that around the switching point between the heating and cooling phases in both scenarios, the RTS transitions were well predicted, as shown in Fig. 19 and Fig. 20. Some broad ''no change'' areas, such as in Fig. 19, during 700 to 850 seconds and during 1150 to 1450 seconds, and in Fig. 20, during 1510 to 1550 seconds and during 1650 to 1700 seconds, were well predicted. Also, many fine details of the RTS were well predicted, such as in the second cooling phase in Fig. 19 and the first heating phase in Fig. 20.

In Scenario I, the TTCL mean prediction accuracy of the MLP and RF classifiers reached 0.50 and 0.50, respectively. In Scenario II, the TTCL mean prediction accuracy of the MLP and RF classifiers reached 0.45 and 0.38, respectively. Since the number of classes is relatively large (nine), the prediction result is not bad.

IV. DISCUSSION

In the first cooling phase in Fig. 20, the air temperature did not show a monotonous downward trend after an abrupt drop and even got an increment. Remarkably, even the ambient air temperature got an increment, the RTS had no ''hotter'' and was mostly ''colder'' during this period as mentioned above. If the RTS were simply assessed by measuring the ambient air temperature trend, a big mistake would be caused.

As we mentioned above, the F1-score of the ''no change'' RTS are relatively lower than the F1-score of the ''hotter'' or ''colder'' RTS. The reason is considered to be the potential neglect of certain subtle thermal sensation changes under gradual heating or cooling phases and cause inaccurate RTSV under such a short voting interval (20 seconds).

In the RTS classification, the class imbalance problem was not severe since the respective total durations of the ''hotter,'' ''colder,'' and ''no change'' RTS were not so much imbalanced. In this investigation, the authors selected a modest value (20 seconds) for the duration of the ''hotter'' and ''colder'' RTSV. Different ''hotter'' and ''colder'' RTSV duration may lead to different results.

Moreover, the subjects felt ''cozy'' at the beginning of the experiment in Fig. 19 and Fig. 20 but felt ''cold'' in the first rapid cooling phase. However, the air temperature in the first rapid cooling phase was no higher than that at the beginning of the experiment, indicating that the ATS does not monotonically depend on the air temperature but also influenced by the context.

A. EARLY WARNING MECHANISM OF THE 9-POINT TTCS

When the subjects were in ''cozy'' TCL in the heating or cooling phases, after some time, the TCL transited to ''hot'' or ''cold'' due to continuous heating or cooling effects. The significance of the RTS is that the accurate RTS prediction can contribute to accurate ''cozy to hot'' or ''cozy to cold'' TTCL predictions and generate early warnings of running into ''hot'' or ''cold'' TCL. For instance, in Fig. 20, in the rapid cooling phase, the subject's TCL was still ''cozy'' after the abrupt temperature drop and finally reached ''cold.'' During this period, the RTS was mostly successfully predicted as ''colder.''

B. LIMITATIONS

This study has some limitations. First, since the 3-point TCS is derived from the 7-point ATSS, the ''cozy'' TCL contains the ''warm,'' ''neutral,'' and ''cool'' ATS, the ''cozy to hot'' or ''cozy to cold'' TTCL does not exclusively mean the TCL is getting away from ''cozy'' and may cause ambiguities. For instance, suppose an occupant's TTCL is ''cozy to hot'', but the original ATSV is ''cool,'' the real ATS transition is from ''cool'' to ''neutral,'' namely, it is towards ''cozy.'' However, it has no negative impact on our theory. For instance, as we mentioned before, in winter, suppose an occupant is staying in an air-conditioning room with the heating system working on, and the occupant's current TTCL is ''cozy to hot.'' In that case, even the occupant's current ATSV is ''cool,'' we can also stop heating the room to keep the occupant in comfortably cool state and even save more energy compared with the case in which the TTCL is ''cozy to hot'' and the ATSV is ''warm.''

Second, in this experiment, since the 3-point RTSS only has three categories (''hotter,'' ''colder,'' and ''no change''),

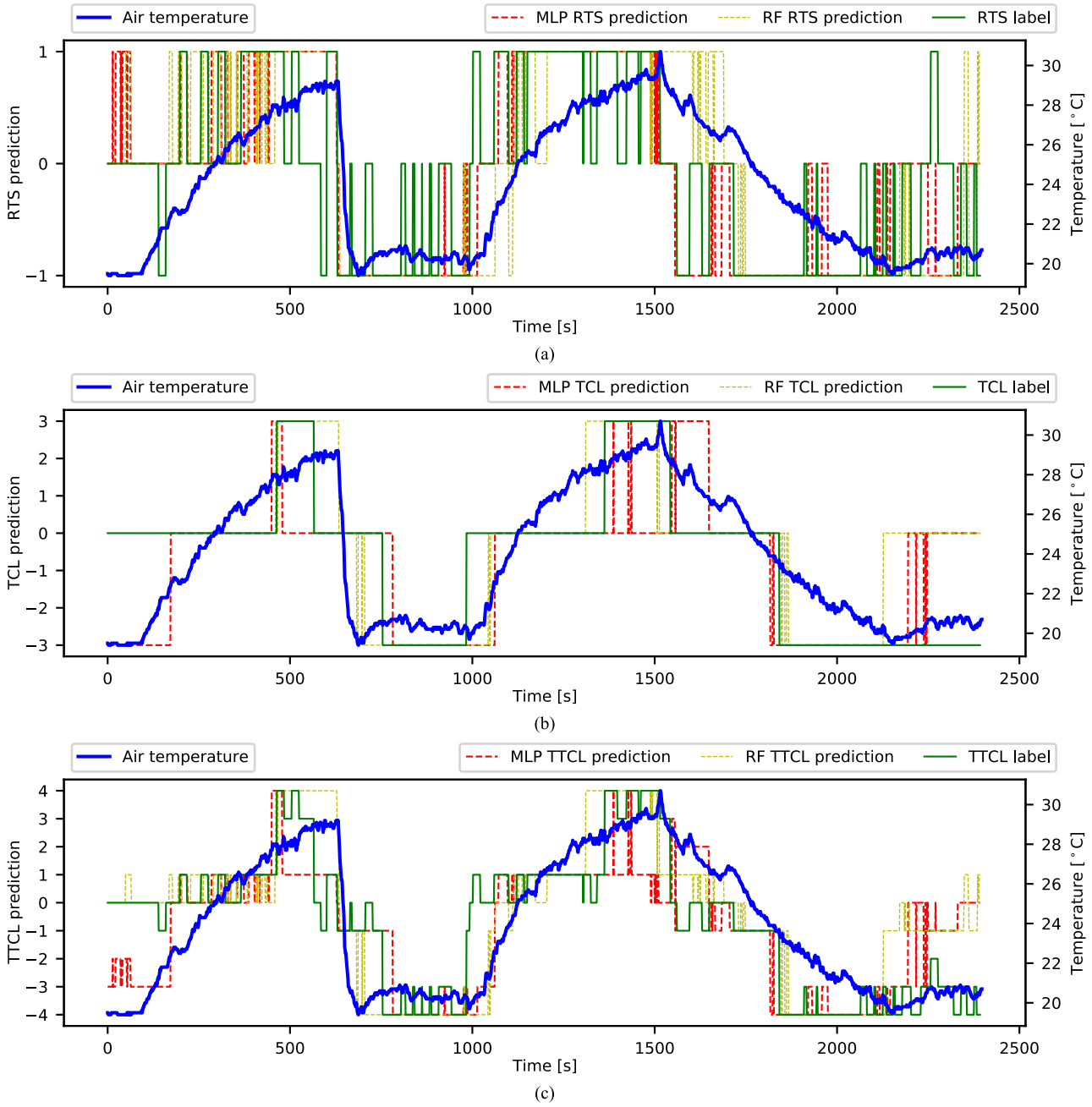

FIGURE 20. Prediction results of the RTS, the TCL, and the TTCL (Scenario II & Subject 4).

it is only possible for qualitative analysis (classification). A very slight "hotter" or "colder" RTS might not last for 20 seconds long and cause possible inaccurate RTS acquisition. In the future study, it could be possible to upgrade the Relative Thermal Sensation Scale to include more categories, e.g., the 7-point RTSS: "much colder," "colder," "slightly colder," "no change," "slightly hotter," "hotter," "much hotter." Then, quantitative analysis becomes possible since continuous RTS can be approximately represented, and regression analysis becomes possible.

Third, as for the TCL evaluation, the authors used a relatively simple method since it is not the key point of this study, the prediction accuracy is tolerantly fair. Many existing studies have focused on thermal comfort evaluation [12], [33] or thermal preference evaluation [30] and got good results. It is possible to get better prediction results by using more features.

Moreover, though both the rapid and gradual cooling phases and the gradual heating phase were investigated, the rapid heating phase was not investigated in this study.

TABLE 5. Confusion matrix, support (the number of actual occurrences of each category), precision, recall, and F1-score of the RTS classification.

Scenario	Subject	Model	Category	Confusion matrix			Support	Precision	Recall	F1-score
				colder	no change	hotter				
I	1	MLP	colder	406	101	18	525	0.77	0.77	0.77
			no change	100	352	356	808	0.54	0.44	0.48
			hotter	24	194	842	1060	0.69	0.79	0.74
		RF	colder	232	183	110	525	0.42	0.44	0.43
			no change	216	214	378	808	0.45	0.26	0.33
			hotter	103	79	878	1060	0.64	0.83	0.72
	2	MLP	colder	684	52	148	884	0.83	0.77	0.80
			no change	93	133	421	647	0.34	0.21	0.26
			hotter	47	209	607	863	0.52	0.70	0.60
		RF	colder	710	16	158	884	0.87	0.80	0.83
			no change	73	167	407	647	0.48	0.26	0.34
			hotter	35	164	664	863	0.54	0.77	0.63
	3	MLP	colder	524	207	2	733	0.64	0.71	0.67
			no change	282	264	286	832	0.45	0.32	0.37
			hotter	16	120	693	829	0.71	0.84	0.77
		RF	colder	576	157	0	733	0.55	0.79	0.65
			no change	437	151	244	832	0.38	0.18	0.24
			hotter	36	94	699	829	0.74	0.84	0.79
II	4	MLP	colder	688	162	16	866	0.71	0.79	0.75
			no change	256	406	223	885	0.62	0.46	0.53
			hotter	31	88	523	642	0.69	0.81	0.75
		RF	colder	722	71	73	866	0.69	0.83	0.75
			no change	285	243	357	885	0.52	0.27	0.36
			hotter	43	153	446	642	0.51	0.69	0.59
	5	MLP	colder	320	214	0	534	0.63	0.60	0.61
			no change	182	516	440	1138	0.56	0.45	0.50
			hotter	8	198	515	721	0.54	0.71	0.61
		RF	colder	226	111	197	534	0.27	0.42	0.33
			no change	427	407	304	1138	0.45	0.36	0.40
			hotter	199	384	138	721	0.22	0.19	0.20
	6	MLP	colder	378	257	52	687	0.83	0.55	0.66
			no change	77	406	358	841	0.40	0.48	0.44
			hotter	0	345	521	866	0.56	0.60	0.58
		RF	colder	316	228	143	687	0.67	0.46	0.54
			no change	101	449	291	841	0.44	0.53	0.48
			hotter	56	340	470	866	0.52	0.54	0.53

Lastly, As this study is focused on personalized thermal comfort evaluation and belongs to non-statistical analysis, a relatively small subject sample size (six subjects) was adopted. Even though the results are significant, a larger subject sample size would enhance the validity of the results.

V. CONCLUSION

In this paper, the authors exclusively proposed the concept of RTS as a complementary index for traditional thermal comfort models and proposed a real-time RTS evaluation method by measuring the skin/clothes temperatures of ten local body segments. The significance of the RTS is that it does not always comply with the ambient air temperature trend. For instance, when the ambient air temperature is ascending, the subject can also obtain a "colder" RTS due to the previous context. The RTS brings new insight for transient-state thermal comfort evaluation. The RTS provides the ordinary thermal comfort model with another dimension to form a complex thermal comfort model. By incorporating the 3-point RTSS into the 3-point TCS, the 9-point TTCS was derived, which has the ability to both predict the current thermal comfort and the thermal sensation variation trend. The authors used an MLP classifier and an RF classifier to predict the RTS and TCL. For the RTS evaluation, in Scenario I, the MLP and RF classifiers reached an average accuracy of 0.63 and 0.60, respectively; in Scenario II, the MLP and RF classifiers reached an accuracy of 0.60 and 0.48, respectively. Due to the fact that the 9-point TTCS is the combination of the 3-point TCS and the 3-point RTSS, the TTCL prediction accuracy reached the lowest. The 9-point TTCS can provide an early warning mechanism for thermal discomfort. The miniaturization of temperature sensors and the non-intrusive temperature measurements like the infrared cameras facilitate practical applications in the future.

ACKNOWLEDGMENT

The authors would like to thank Reina Aizawa and Chikato Yokoyama for useful discussions and suggestions. Experimental apparatus support from Tokyo Gas Company Ltd., is acknowledged.

REFERENCES

[1] *Thermal Environmental Conditions for Human Occupancy*, ANSI/ASHRAE Standard 55-2017, ASHRAE Inc., 2017, vol. 2017, p. 66.
[2] C. D. Korkas, S. Baldi, I. Michailidis, and E. B. Kosmatopoulos, "Occupancy-based demand response and thermal comfort optimization in microgrids with renewable energy sources and energy storage," *Appl. Energy*, vol. 163, pp. 93–104, Feb. 2016.
[3] C. D. Korkas, S. Baldi, and E. B. Kosmatopoulos, "Grid-connected microgrids: Demand management via distributed control and human-in-the-loop optimization," in *Advances in Renewable Energies and Power Technologies*, I. Yahyaoui, Ed. Amsterdam, The Netherlands: Elsevier, Jan. 2018, pp. 315–344.
[4] C. D. Korkas, S. Baldi, I. Michailidis, and E. B. Kosmatopoulos, "Intelligent energy and thermal comfort management in grid-connected microgrids with heterogeneous occupancy schedule," *Appl. Energy*, vol. 149, pp. 194–203, Jul. 2015.
[5] R. Yao, B. Li, and J. Liu, "A theoretical adaptive model of thermal comfort–adaptive predicted mean vote (aPMV)," *Building Environ.*, vol. 44, no. 10, pp. 2089–2096, Oct. 2009.
[6] M. A. Humphreys and J. F. Nicol, "The validity of ISO-PMV for predicting comfort votes in every-day thermal environments," *Energy Buildings*, vol. 34, no. 6, pp. 667–684, Jul. 2002.
[7] T. Chaudhuri, Y. C. Soh, S. Bose, L. Xie, and H. Li, "On assuming mean radiant temperature equal to air temperature during PMV-based thermal comfort study in air-conditioned buildings," in *Proc. 42nd Annu. Conf. IEEE Ind. Electron. Soc. (IECON)*, Oct. 2016, pp. 7065–7070.
[8] K. Fabbri, "Thermal comfort evaluation in kindergarten: PMV and PPD measurement through datalogger and questionnaire," *Building Environ.*, vol. 68, pp. 202–214, Oct. 2013.
[9] S. T. Mors, J. L. M. Hensen, M. G. L. C. Loomans, and A. C. Boerstra, "Adaptive thermal comfort in primary school classrooms: Creating and validating PMV-based comfort charts," *Building Environ.*, vol. 46, no. 12, pp. 2454–2461, Dec. 2011.
[10] Y. Yao, Z. Lian, W. Liu, and Q. Shen, "Experimental study on skin temperature and thermal comfort of the human body in a recumbent posture under uniform thermal environments," *Indoor Built Environ.*, vol. 16, no. 6, pp. 505–518, Dec. 2007.
[11] H. Zhang, E. Arens, C. Huizenga, and T. Han, "Thermal sensation and comfort models for non-uniform and transient environments: Part I: Local sensation of individual body parts," *Building Environ.*, vol. 45, no. 2, pp. 380–388, Feb. 2010.
[12] J.-H. Choi and D. Yeom, "Study of data-driven thermal sensation prediction model as a function of local body skin temperatures in a built environment," *Building Environ.*, vol. 121, pp. 130–147, Aug. 2017.
[13] S. I. U. H. Gilani, M. H. Khan, and W. Pao, "Thermal comfort analysis of PMV model prediction in air conditioned and naturally ventilated buildings," *Energy Procedia*, vol. 75, pp. 1373–1379, Aug. 2015.
[14] K. N. Nkurikiyeyezu, Y. Suzuki, and G. F. Lopez, "Heart rate variability as a predictive biomarker of thermal comfort," *J. Ambient Intell. Humanized Comput.*, vol. 9, no. 5, pp. 1465–1477, Oct. 2018.
[15] Z. Wang and R. Matsuhashi, "Research on thermal comfort by analyzing LF/HF value and heat flow rate," *J. Soc. Energy Resour.*, vol. 40, no. 5, pp. 154–159, 2019.
[16] Y. Yao, Z. Lian, W. Liu, C. Jiang, Y. Liu, and H. Lu, "Heart rate variation and electroencephalograph—The potential physiological factors for thermal comfort study," *Indoor Air*, vol. 19, no. 2, pp. 93–101, Apr. 2009.
[17] T. Chaudhuri, D. Zhai, Y. C. Soh, H. Li, and L. Xie, "Random forest based thermal comfort prediction from gender-specific physiological parameters using wearable sensing technology," *Energy Buildings*, vol. 166, pp. 391–406, May 2018.
[18] M. Beggiato, F. Hartwich, and J. Krems, "Using smartbands, pupillometry and body motion to detect discomfort in automated driving," *Frontiers Hum. Neurosci.*, vol. 12, p. 338, Sep. 2018.
[19] E. Schmidt and A. C. Bullinger, "Mitigating passive fatigue during monotonous drives with thermal stimuli: Insights into the effect of different stimulation durations," *Accident Anal. Prevention*, vol. 126, pp. 115–121, May 2019.
[20] H. Metzmacher, D. Wölki, C. Schmidt, J. Frisch, and C. van Treeck, "Real-time human skin temperature analysis using thermal image recognition for thermal comfort assessment," *Energy Buildings*, vol. 158, pp. 1063–1078, Jan. 2018.
[21] A. C. Cosma and R. Simha, "Thermal comfort modeling in transient conditions using real-time local body temperature extraction with a thermographic camera," *Building Environ.*, vol. 143, pp. 36–47, Oct. 2018.
[22] J. Ranjan and J. Scott, "ThermalSense: Determining dynamic thermal comfort preferences using thermographic imaging," in *Proc. ACM Int. Joint Conf. Pervas. Ubiquitous Comput.*, Sep. 2016, pp. 1212–1222.
[23] J. Miura, M. Demura, K. Nishi, and S. Oishi, "Thermal comfort measurement using thermal-depth images for robotic monitoring," *Pattern Recognit. Lett.*, vol. 137, pp. 1–6, Sep. 2019.
[24] Z. S. Zomorodian, M. Tahsildoost, and M. Hafezi, "Thermal comfort in educational buildings: A review article," *Renew. Sustain. Energy Rev.*, vol. 59, pp. 895–906, Jun. 2016.
[25] A. Martínez-Molina, I. Tort-Ausina, S. Cho, and J.-L. Vivancos, "Energy efficiency and thermal comfort in historic buildings: A review," *Renew. Sustain. Energy Rev.*, vol. 61, pp. 70–85, Aug. 2016.
[26] R. F. Rupp, N. G. Vásquez, and R. Lamberts, "A review of human thermal comfort in the built environment," *Energy Buildings*, vol. 105, pp. 178–205, Oct. 2015.
[27] M. Taleghani, M. Tenpierik, S. Kurvers, and A. van den Dobbelsteen, "A review into thermal comfort in buildings," *Renew. Sustain. Energy Rev.*, vol. 26, pp. 201–215, Oct. 2013.
[28] R. Zhao, "Investigation of transient thermal environments," *Building Environ.*, vol. 42, no. 12, pp. 3926–3932, Dec. 2007.
[29] R. J. de Dear and G. S. Brager, "Thermal comfort in naturally ventilated buildings: Revisions to ASHRAE standard 55," *Energy Buildings*, vol. 34, no. 6, pp. 549–561, Jul. 2002.
[30] D. Li, C. C. Menassa, and V. R. Kamat, "Non-intrusive interpretation of human thermal comfort through analysis of facial infrared thermography," *Energy Buildings*, vol. 176, pp. 246–261, Oct. 2018.
[31] N. Djongyang, R. Tchinda, and D. Njomo, "Thermal comfort: A review paper," *Renew. Sustain. Energy Rev.*, vol. 14, no. 9, pp. 2626–2640, 2010.
[32] B. W. Olesen and G. S. Brager, "A better way to predict comfort: The new ASHRAE standard 55-2004," *ASHRAE J.*, vol. 46, no. 8, pp. 20–28, Aug. 2004.
[33] A. Ghahramani, G. Castro, S. A. Karvigh, and B. Becerik-Gerber, "Towards unsupervised learning of thermal comfort using infrared thermography," *Appl. Energy*, vol. 211, pp. 41–49, Feb. 2018.
[34] K. B. Velt and H. A. M. Daanen, "Thermal sensation and thermal comfort in changing environments," *J. Building Eng.*, vol. 10, pp. 42–46, Mar. 2017.
[35] H. B. Rijal, M. A. Humphreys, and J. F. Nicol, "Adaptive model and the adaptive mechanisms for thermal comfort in Japanese dwellings," *Energy Buildings*, vol. 202, Nov. 2019, Art. no. 109371.
[36] R. Thapa, H. B. Rijal, and M. Shukuya, "Field study on acceptable indoor temperature in temporary shelters built in nepal after massive earthquake 2015," *Building Environ.*, vol. 135, pp. 330–343, May 2018.
[37] S. Shahzad and H. B. Rijal, "Preferred vs neutral temperatures and their implications on thermal comfort and energy use: Workplaces in Japan, Norway and the UK," *Energy Procedia*, vol. 158, pp. 3113–3118, Feb. 2019.
[38] H. B. Rijal, M. A. Humphreys, and J. F. Nicol, "Towards an adaptive model for thermal comfort in Japanese offices," *Building Res. Inf.*, vol. 45, no. 7, pp. 717–729, Oct. 2017.
[39] S. C. Jiang, N. Ma, H. J. Li, and X. X. Zhang, "Effects of thermal properties and geometrical dimensions on skin burn injuries," *Burns*, vol. 28, no. 8, pp. 713–717, Dec. 2002.
[40] M. Kashcooli, M. R. Salimpour, and E. Shirani, "Heat transfer analysis of skin during thermal therapy using thermal wave equation," *J. Thermal Biol.*, vol. 64, pp. 7–18, Feb. 2017.
[41] Y. Kurazumi, T. Tsuchikawa, J. Ishii, K. Fukagawa, Y. Yamato, and N. Matsubara, "Radiative and convective heat transfer coefficients of the human body in natural convection," *Building Environ.*, vol. 43, no. 12, pp. 2142–2153, Dec. 2008.
[42] S. Sim, M. Koh, K. Joo, S. Noh, S. Park, Y. Kim, and K. Park, "Estimation of thermal sensation based on wrist skin temperatures," *Sensors*, vol. 16, no. 4, p. 420, Mar. 2016.
[43] C. Bergmeir and J. M. Benítez, "On the use of cross-validation for time series predictor evaluation," *Inf. Sci.*, vol. 191, pp. 192–213, May 2012.

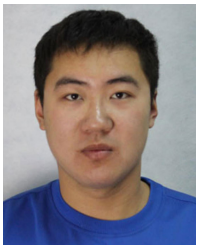

ZIYANG WANG received the B.E. degree from the Beijing University of Chemical Technology, Beijing, China, in 2016, and the M.S. degree in electrical engineering and information systems from The University of Tokyo, Tokyo, Japan, in 2019, where he is currently pursuing the Ph.D. degree.

He joined Silver Egg Technology Company Ltd., as an Intern, in 2018. He joined the Department of Electrical Engineering and Information Systems, The University of Tokyo, as a Research Assistant, in 2019. His research interests include thermal comfort evaluation, machine learning, and wearable cooling device.

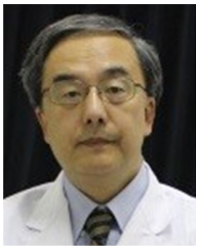

HIROSHI ONODERA received the M.S. and Ph.D. degrees in medical science from the Tohoku University School of Medicine, Sendai, Japan, in 1985.

From 1998 to 2005, he was an Associate Professor with the Department of Neurology, Tohoku University School of Medicine. Since 2014, he has been a Project Professor with the Photon Science Center and Electrical Engineering, Graduate School of Engineering, The University of Tokyo. His research interests include three-dimensional visualization of biological samples and optogenetics produced clinical benefits for cancer diagnosis and rehabilitation fields.

Dr. Onodera is a member of The Japanese Society of Internal Medicine, The Japanese Society of Neurology, and The Robotics Society of Japan.

RYUJI MATSUHASHI received the B.E. and Ph.D. degrees in electronics from The University of Tokyo, Tokyo, Japan, in 1985 and 1990, respectively.

From 1990 to 1993, he was a Research Associate with the Department of Geosystem Engineering, Faculty of Engineering, The University of Tokyo, where he has been an Associate Professor, since 1994. Since 1999, he has been an Associate Professor with the Graduate School of Frontier Sciences, Institute of Environmental Studies, The University of Tokyo. Since 2003, he has been a Professor with the Institute of Environmental Studies, The University of Tokyo. Since 2011, he has been a Professor with the Electrical Engineering and Information Systems, Graduate School of Engineering, The University of Tokyo. His research interests include analysis of energy systems and global environmental issues produced various books and papers.

Dr. Matsuhashi is currently a member of the Japan Society of Energy and Resources, the Institute of Electrical Engineers of Japan, and the Japan Institute of Energy.